



## Accurate nanoparticle size determination using electrical mobility measurements in the step and scan modes

Kaleb Duelge, George Mulholland, Michael Zachariah & Vincent A. Hackley

To cite this article: Kaleb Duelge, George Mulholland, Michael Zachariah & Vincent A. Hackley (2022) Accurate nanoparticle size determination using electrical mobility measurements in the step and scan modes, *Aerosol Science and Technology*, 56:12, 1096-1113, DOI: [10.1080/02786826.2022.2128986](https://doi.org/10.1080/02786826.2022.2128986)

To link to this article: <https://doi.org/10.1080/02786826.2022.2128986>

 View supplementary material [↗](#)

 Published online: 12 Oct 2022.

 Submit your article to this journal [↗](#)

 Article views: 179

 View related articles [↗](#)

 View Crossmark data [↗](#)

 Citing articles: 1 View citing articles [↗](#)



## Accurate nanoparticle size determination using electrical mobility measurements in the step and scan modes

Kaleb Duelle<sup>a,b</sup> , George Mulholland<sup>a,b</sup> , Michael Zachariah<sup>b,c</sup> , and Vincent A. Hackley<sup>a</sup>

<sup>a</sup>National Institute of Standards and Technology, Gaithersburg, Maryland, USA; <sup>b</sup>Department of Chemistry, University of Maryland, College Park, Maryland, USA; <sup>c</sup>Departments of Chemical Engineering and Materials Science, University of California, Riverside, California, USA

### ABSTRACT

A critical and extensive comparison was made between differential mobility analysis (DMA) measurements of the mean diameter of monodisperse gold nanoparticles (AuNPs), based on step-voltage mode and the more commonly used scan-voltage mode (commercially known as scanning mobility particle sizer, SMPS). Under specific conditions including a long scan time, the difference between mean diameters measured by the two modes of operation was less than the expanded combined uncertainty (95% confidence interval) for the step-voltage mode. In addition, a comparison was made between two different calibration methods for DMA: the use of a certified nanoparticle size standard (artifact) versus a direct measurement of the sheath flow rate. Important variables and limitations for accurate measurements by the scan-voltage method were identified and evaluated. The mean size shifts to smaller electrical mobility diameters as the scan time is reduced and the scan mode is unable to measure sufficient points across the peak of very narrow size distributions, leading to systematic errors. The use of a calibration particle corrects for the flow and DMA column geometric effects and was found to minimize the effect of a reduced scan time. A methodology is presented for the use of these AuNPs and other monodisperse calibration particles for accurately calibrating SMPS instruments for the measurement of the electrical mobility diameter distribution.

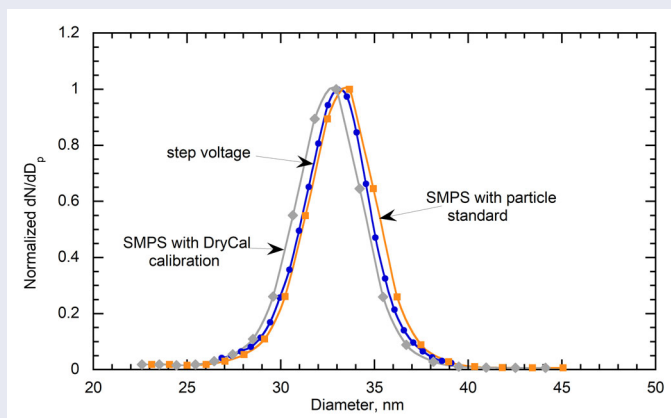
### ARTICLE HISTORY

Received 16 June 2022  
Accepted 14 September 2022

### EDITOR

Jason Olfert

### GRAPHICAL ABSTRACT



## Introduction

Nanoparticle “size,” typically a method-defined measurement and frequently based on the diameter of an equivalent sphere, is an important characteristic that impacts particle transport properties, such as mobility, diffusion, friction, coagulation, and charging. Size also

plays an important role in optically active materials and is a critical factor in biodistribution. It is therefore important to accurately measure the size of nanoparticles, which is why size standards are relied on heavily in research and industry. A common method for certifying standards in industry is based on

**CONTACT** Vincent A. Hackley [vince.hackley@nist.gov](mailto:vince.hackley@nist.gov) 100 Bureau Dr., MS 8520, Gaithersburg, MD 20899-8520, USA.

Supplemental data for this article can be accessed online at <https://doi.org/10.1080/02786826.2022.2128986>

© 2022 American Association for Aerosol Research

electron microscopy (Particle Technology Technical Notes and Reference Guide – Strategies and Procedures for Bead Optimization 2018). In some cases, the known and unknown particles are mixed and deposited together on a microscope grid. Well-characterized methods, such as light scattering (Mulholland et al. 1985), the calibrated atomic force microscope of the National Institute of Standards and Technology (NIST) (Dixson et al. 1999), and electro-gravitational aerosol balance (Takahata, Sakurai, and Ehara 2020), where the key uncertainty terms have been calculated, can be used for primary certification. It is also ideal for a method to be traceable, where a direct connection is made to an international system of units (SI): most often the meter, but potentially the kilogram if particle mass or volume and density are determined.

Several nanoparticle size artifacts are available for use. Within the size range from 10 nm to 100 nm, there are calibration particles available from various sources consisting of, for example, polystyrene, silica, gold, and silver. Monodisperse polystyrene spheres traceable to the SI for nominal sizes of 60 nm and 100 nm are available from NIST. Gold nanoparticles (AuNPs) are of special interest because of their biocompatibility and optical properties (Elahi, Kamali, and Baghersad 2018). Reference (citrate stabilized) AuNP calibrants with nominal sizes of 10 nm (RM 8011), 30 nm (RM 8012), and 60 nm (RM 8013) and coefficients of variation (CVs, the standard deviation of the size distribution divided by the mean) of 5% to 8% were issued by NIST in 2007. The mean particle diameter was determined by differential mobility analysis (DMA, which includes an electrostatic classifier and a condensation particle counter), scanning electron microscopy (SEM), transmission electron microscopy (TEM), atomic force microscopy (AFM), dynamic light scattering (DLS), and small angle X-ray scattering (SAXS), and the values obtained by each method were reported on the certificate. These values were not traceable to SI units, nor was a complete uncertainty budget included. Even with these limitations, the 30 nm and 60 nm particles were in high demand and the supply was exhausted. Replacement candidate reference materials (RMs) produced by citrate reduction of a gold chloride solution are being characterized by a variety of measurements including DMA. In this article, we examine electrical mobility measurements conducted on these candidate RMs in step-voltage mode, the calibration of the DMA by 60 nm polystyrene standard reference material (SRM) 1964, and a quantitative uncertainty budget.

DMA is an aerosol sizing technique that has been used extensively for particle measurements related to combustion (Lamberg et al. 2018; Choi, Myung, and Park 2014), climate (Gibson, Hudson, and Grassian 2006; Smith et al. 2010), and particle engineering (Tsai et al. 2011; Guha et al. 2012). DMA has also been employed in the measurement of particle size standards. It has been used to certify NIST standard reference material (SRM) 1963 (Mulholland, Bryner, and Croarkin 1999), 1963a, and 1964 (Mulholland et al. 2006). DMA was also one of many techniques used to assign reference values to NIST RMs 8011, 8012, and 8013, as previously mentioned. DMA is not generally used as a primary calibration technique because of the uncertainty in the flow dynamics where the aerosol inlet flow meets the sheath flow. In addition, there may be minor fringe effects on the electric field used for separation. DMA is more commonly used as a secondary calibration technique, where the known size of a primary standard is used for calibration and an unknown particle is measured and is traceable to the primary standard. DMA is suited for these measurements because it is highly reproducible, yields a number-weighted distribution, can measure high particle number counts with correspondingly higher statistical significance, the size resolution is easily controllable, and it has a well-defined electrical mobility transfer function (the probability that particles of given electrical mobility will exit the DMA column).

DMA is often operated in one of two modes: step-voltage or scan-voltage. The step-voltage mode steps through the voltage range, spending a specified amount of time at each selected voltage (with some equilibration time before and after each step). Each voltage corresponds to a specific electrical mobility (which is related to the particle diameter) and the particles exiting the DMA column are counted using a condensation particle counter (CPC). Historically, DMA has been used in the step-voltage mode because it is straightforward to determine the particle diameter from measurements of number concentration versus voltage. This is the method that has been used in the previous certification of NIST SRMs for particle size.

However, the step-voltage mode is not suited to all aerosols. Some aerosol size distributions change rapidly, on the order of the amount of time needed to step through the full population of sizes. Due to this limitation, the scan-voltage mode was developed to allow for more rapid measurements (Wang and Flagan 1990). The scan-voltage mode, in which the number concentration of the aerosol exiting the DMA

**Table 1.** Summary of various nanomaterials used.

Particle	Nominal diameter (nm)	Use
RM30	30	Comparison between step-voltage and SMPS
RM60	60	Comparison between step-voltage and SMPS
SRM 1964	60	Calibration
SRM 1963a	100	Demonstrate SMPS size interval limitation (Figure 9)
Ted Pella AuNPs	60	Test measurements of SMPS scan time and delay time (Tables 8 and 9)

is continuously monitored with a CPC as the voltage is continuously ramped, is widely referred to as scanning mobility particle sizer (SMPS). The SMPS takes advantage of the inherent dead time in a DMA system: the time it takes the detector to reach a steady-state concentration after a voltage change, which is essentially wasted for each step of a step-voltage mode measurement. If this dead time is known, the voltage can be changed before the first size-selected particles reach the detector. For the SMPS model used here, the voltage is varied exponentially, a well-known time-constant defines the transport from the entrance of the DMA column to the detector, and each detector signal is thereby related to a particular diameter in the limit of a long scan time. This significantly reduces the measurement time for broad size distributions, such as the entire size range of the so-called “long” DMA column: 10 nm to 1000 nm. Using the step-voltage mode, a measurement would typically take from 30 min to 45 min to complete, while the SMPS (over the same 10 V – 10,000 V range) can be completed in only 30 s. Over time the SMPS has become ubiquitous due to its commercial availability, speed, and ease of use. Some recent results of modeled particle behavior in the step and scan mode are covered in the discussion.

The accuracy of the SMPS mobility diameter measurements is of interest due to its broad use in the aerosol field and adoption in nanotechnology applications. Initial investigations with the SMPS indicated that the size distributions of 23.2 nm ammonium sulfate aerosol with a CV of 1% measured with an 80 s scan time were nominally identical to the step-voltage mode results (Wang and Flagan 1990); however, data have not been presented for measurements of size standards. Here, we investigate a simple application of the SMPS: the measurement of the number average diameter of a narrow size distribution (CV less than 15%). In this case, the effects of multiple charging and size-dependent losses are minor. We compare the mean diameter obtained by step mode and SMPS when we use 60 nm SRM 1964 to calibrate both configurations (the voltage was also independently calibrated for both configurations). In addition, we independently calibrate the SMPS measurements using

a direct measurement of the sheath flow. We investigate the effects of scan time and delay time on the SMPS measurement. We compare the step and scan mode using uncalibrated measurements with identical hardware, making alternate measurements within a single day. The step-voltage mode remains the operational mode of choice for size certification measurements. One objective is to assess whether the SMPS can be calibrated using the proposed AuNPs or existing polystyrene latex (PSL) spheres.

## Materials and methods<sup>1</sup>

### Chemicals and materials

NIST candidate AuNP RMs, nominally 30 nm and 60 nm diameter, are denoted here as RM30 and RM60, respectively. The source materials were prepared to NIST specifications by BBI Solutions (Crumlin, UK). These candidate RMs are currently in production at NIST and therefore the value assignments provided in this work are to be considered preliminary in nature. NIST SRM 1963a, nominally 100 nm PSL, was used. SRM 1964, nominally 60 nm PSL, was used for instrument calibration. Ultrapure deionized (DI) water (18.2 MΩ cm) was used for sample preparation (Model 2121AL, Aqua Solutions, Jasper, GA, USA). Ammonium acetate (>99.99%) was purchased from Sigma-Aldrich (St. Louis, MO, USA) and nominally 60 nm citrate stabilized AuNPs were purchased from Ted Pella (Redding, CA, USA). These particles were used for practice measurements and for investigation of the effect of SMPS scan and delay times. RM30 and RM60 are slightly nonspherical as shown in Figures 3 and 4. In this case, the electrical mobility diameter is measured, which is the diameter of a sphere that has the same electrical mobility as the nonspherical particle (Table 1).

<sup>1</sup>Commercial equipment, instruments, or materials identified in this paper are intended to specify the experimental procedure adequately. Their use is not a recommendation or endorsement by the National Institute of Standards and Technology, nor does it imply that the materials or equipment identified are necessarily the best available for the purpose.

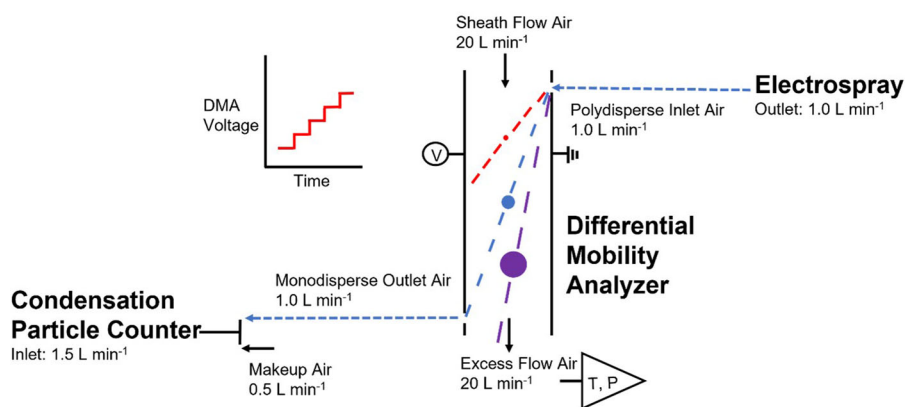


Figure 1. Schematic of step-voltage mode measurements.

### Sample preparation

AuNP suspensions were prepared by centrifuging 1 mL stock (nominally  $50 \text{ mg kg}^{-1} \text{ Au}$ ) in a lo-bind microcentrifuge tube (Eppendorf, Hamburg, Germany) at 3900 rcf (relative centrifugal force) for 12 min. The supernatant ( $950 \mu\text{L}$ ) was removed and replaced with  $300 \mu\text{L}$  of  $0.15 \text{ g L}^{-1}$  ammonium acetate, a volatile salt that leaves minimal residual on the particles after drying, and the suspension was vortexed for 10 s. AuNPs were measured between 0 h to 5 h after buffer exchange. PSL suspensions were prepared by adding  $100 \mu\text{L}$  of bath sonicated stock (5 min) to 1 mL DI water and filtered ( $0.2 \mu\text{m}$ , Whatman, Maidstone, UK). Briefly,  $50 \mu\text{L}$  of the filtered suspension was added to  $450 \mu\text{L}$  of  $0.15 \text{ g L}^{-1}$  ammonium acetate.

### Step-voltage

The DMA system used here has been reported previously (Duelge et al. 2020). Briefly, the system consists of a spray source, a DMA column, and a particle counter. In this case, an electro spray source (Model 3480, TSI, Shoreview, MN, USA) was used. The long DMA column (Model 3081, TSI) was used for measurements of RM30, RM60, and SRM 1964. The nano DMA column (Model 3085, TSI) was used for measurements of salt particles generated by the electro spray (explained further in the paragraph before Equation (11)). The electro spray was set to 2.5 kV to 3.5 kV with a resulting current of  $-150 \text{ nA}$  to  $-250 \text{ nA}$ . The pressurized sample cell was set to 26 kPa (3.7 psi). Particles were sprayed through a  $40 \mu\text{m}$  inner diameter fused silica capillary (Part CB23056, TSI). The aerosol flow rate was  $1 \text{ L min}^{-1}$  air and brought to a Boltzmann charge distribution with a Po-210 alpha-emitter (Model P-2042, TSI). The measurement was made in “overpressure mode,” in which the flow to

the condensation particle counter (CPC, Model 3776, TSI) was pushed by the aerosol and sheath flow. The voltage for the DMA column was set by a Bertan power supply (Model 205B-10R, Spellman, Hauppauge, NY, USA) controlled by a custom LabVIEW code (National Instruments, Austin, TX, USA). The  $20 \text{ L min}^{-1}$  sheath flow was set by an external mass flow controller without recirculation (Model 1480A01334CS1BM, MKS Instruments, Andover, MA, USA). The monodisperse outlet flow from the DMA column was set to  $1.0 \text{ L min}^{-1}$ . The temperature and pressure were measured by an external flow meter (Model 4043, TSI) in-line with the excess flow (details included below). The particles were detected by a CPC with a  $1.5 \text{ L min}^{-1}$  flow rate. A tee fitting was placed at the entrance of the CPC with an attached HEPA filter to compensate the mismatch between the aerosol flow and the CPC flow (see Figure 1). RM30 was measured from 28 nm to 40 nm with 0.5 nm spacing. RM60 was measured from 55 nm to 79 nm with 1 nm spacing. The mode of SRM 1964 was measured from 52 nm to 67 nm with 0.5 nm spacing.

### SMPS

The same electro spray, DMA column, and CPC detector were used for the SMPS measurements. The same external flow meter was used to measure the temperature and pressure. AIM (Aerosol Instrument Manager, TSI) software version 9.0.0.0 was used to make SMPS measurements. The primary differences between step mode and SMPS were the recirculated sheath flow controlled by the electrostatic classifier (Model 3080, TSI) and the resulting “underpressure mode” measurement in which the CPC pulls air through the DMA column with a valve between the electro spray and DMA column (see Figure 2). The

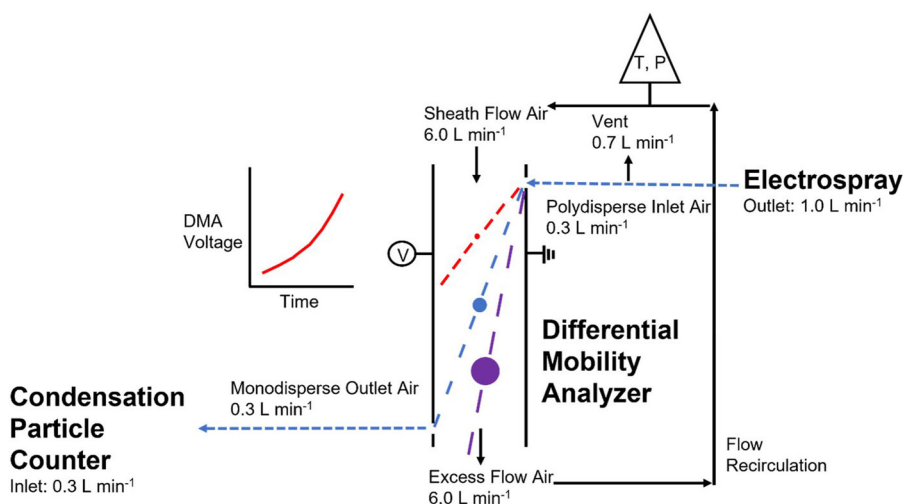


Figure 2. Schematic for SMPS measurements.

CPC was set to  $0.3 \text{ L min}^{-1}$  low flow mode and the sheath flow was set to  $6 \text{ L min}^{-1}$  resulting in the same aerosol-to-sheath flow ratio as the step-voltage mode (1:20). The lower flows were selected because the electrostatic classifier had a maximum sheath flow rate of approximately  $15 \text{ L min}^{-1}$ . A  $0.0508 \text{ cm}$  nozzle size impactor was installed in-line between the electro spray and DMA column. The measurements of RM30 and RM60 were made with a 300 s scan up time and 30 s scan down time. The delay time ( $t_d$ ) is the time required for the aerosol to flow through the DMA column and the tubing connecting to the CPC, and was set to the default value for the measurements of RM30 and RM60: 3.43 s. Initial test measurements were made with alternative 60 nm AuNPs (Ted Pella) to vary measurement times (Table 8) and delay times (Table 9). The software presents the data as diameter versus  $dN/d\log D_p$ , where  $dN/d\log D_p$  is the number size distribution (defined below), which is related to the CPC number concentration by Equations (7) and (9). Prior to calibrating the voltage and the sheath flow, we reverse the process described in the previous sentence, and derive the raw data in terms of voltage (Equation (3)) and number concentration (Equation (7)) that is comparable to the step-voltage measurement. RM30 was measured from 24.1 nm to 46.1 nm with 19 data points. RM60 was measured from 51.4 nm to 85.1 nm with 15 data points. The mode of SRM 1964 was measured from 47.8 nm to 71 nm with 12 data points. The data points were evenly spaced on a logarithmic scale with 64 channels per decade. Choosing a narrow size range and a long scan time reduces the voltage scan rate for the measurement. Additional comparison measurements between step-voltage mode and the SMPS were made of SRM 1963

to demonstrate the limitations of the step width for the SMPS (Figure 9). Finally, step-voltage mode and SMPS measurements were made of the alternative 60 nm AuNPs (Ted Pella) using the same uncalibrated sheath flow (the SMPS recirculating system), using the two calibrated power supplies described below, and the same values for the Cunningham Slip Correction, such that the only primary difference is the mode of changing voltage.

### Differential mobility analysis

The electrical mobility,  $Z_p$ , is determined by the balance of the drag force and the electrostatic force.

$$Z_p = \frac{neC_c(D_p)}{3\pi\mu D_p} \quad (1)$$

where  $n$  is the number of charges,  $e$  is the elementary charge,  $C_c$  is the Cunningham slip correction factor (described below),  $\mu$  is the viscosity of the gas, and  $D_p$  is the mobility diameter. The expression for the peak mobility of a particle exiting the DMA column (Knutson and Whitby 1975) is given by:

$$Z_{p1} = \frac{q_{sh}\ln(r_2/r_1)}{2\pi LV} \quad (2)$$

where  $q_{sh}$  is the sheath flow rate,  $r_2$  is the inner diameter of the outer electrode,  $r_1$  is the outer diameter of the inner electrode,  $L$  is the length of the DMA column from entrance slit to exit slit, and  $V$  is the voltage of the inner electrode. Equations (1) and (2) are combined to determine the mobility diameter from DMA measurements.

$$\frac{D_p}{C_c(D_p)} = \frac{2neVL}{3\mu q_{sh}\ln(r_2/r_1)} \quad (3)$$

DMA measures the number concentration of an aerosol at the detector (CPC) post transport through the DMA column. In the step mode, this measurement,  $N_{\text{CPC}}$ , is a convolution of the size distribution of the aerosol before the DMA column,  $G(Z_p)$ , and the transfer function through the DMA column,  $\Omega(Z_p)$ .

$$N_{\text{CPC}}(V) = \int \Omega(Z_p, V)G(Z_p)dZ_p \quad (4)$$

where  $G(Z_p) = dN/dZ_p$  and  $dN$  is the number concentration of charged particles with electrical mobilities between  $Z_p$  and  $Z_p + dZ_p$ .

Expressing Equation (4) in terms of the size distribution for all the particles entering the DMA column,  $F(D_p) = dN/dD_p$ , one obtains the following equation including a term for particle charging,  $P(D_p)$  (Wiedensohler 1988). In this work, particles with a single positive charge were selected.

$$N_{\text{CPC}}(V) = \int \Omega(Z_{p,+1}V)F(D_p(Z_{p,+1}))P(D_{p,+1}) \left| \frac{dD_{p,+1}}{dZ_{p,+1}} \right| dZ_{p,+1} \quad (5)$$

$$\log_{10}P(D_{p,+1}) = \sum_{i=0}^5 A_i(+1) \left( \log_{10} \frac{D_p}{D_{p,\text{unit}}} \right)^i \quad (6)$$

The  $A_i$  terms  $-2.3484$ ,  $0.6044$ ,  $0.48$ ,  $0.0013$ ,  $-0.1553$ , and  $0.032$  were used respectively for particle with a single positive charge.

Making a standard approximation that all the quantities except the transfer function change slowly with diameter, one obtains the following expression for the diameter size distribution

$$F(D_p) = \left[ N_{\text{CPC}}(V) \left| \frac{C'_c(D_p)}{C_c(D_p)} - \frac{1}{D_p} \right| \right] / [(\delta)(P(D_p))] \quad (7)$$

where  $C'_c(D_p)$  is the derivative of the slip correction with respect to diameter,  $\frac{C'_c(D_p)}{C_c(D_p)} - \frac{1}{D_p}$  is proportional to the term  $\left| \frac{dD_p}{dZ_p} \right|$ , and  $\delta$  is equal to the aerosol flow divided by the sheath flow.

$C_c$  is the Cunningham slip correction factor:

$$C_c = 1 + Kn(\alpha + \beta(\exp(-\gamma/Kn))) \quad (8)$$

where  $\alpha$ ,  $\beta$ , and  $\gamma$  are empirical constants for the slip correction. The SMPS software (AIM) uses 1.142, 0.558, and 0.999, respectively, but we reanalyzed the data using the values 1.165, 0.483, and 0.997, because these terms were determined using particle standards of known size (Kim et al. 2005).  $Kn$  is the Knudsen

number,  $2\lambda/D_p$ , and  $\lambda$  is the mean free path of the gas.

An alternative form for the size distribution is in terms of the logarithmic derivative  $F_1(D_p(Z_p))$ :

$$F_1(D_p) = \frac{dN(D_p)}{d \log D_p} = \frac{dN(D_p)}{dD_p} \bullet D_p \bullet \ln(10) \quad (9)$$

The number average diameter was calculated using the following equation:

$$\bar{D}_p = \frac{\sum_i \left[ (D_{p,i}) \left( \frac{dN_i}{d \log D_{p,i}} \right) (d \log D_{p,i}) \right]}{\sum_i \left[ \left( \frac{dN_i}{d \log D_{p,i}} \right) (d \log D_{p,i}) \right]} \quad (10)$$

Nonvolatile salts (residuals in ultrapure water and colloidal stabilizers) will coat the analyte nanoparticles during droplet evaporation post electrospray. This increase in size was corrected to determine the size of the analyte particles in suspension by measuring the size of salt particles produced by droplets that do not contain AuNPs. From conservation of mass, assuming constant salt packing, one can derive the following equation:

$$\bar{D}_{p,c} = \sqrt[3]{\bar{D}_p^3 - \bar{D}_{p,\text{salt}}^3} \quad (11)$$

$\bar{D}_{p,c}$  is the mean electrical mobility diameter of the particle without the nonvolatile salt coating.  $\bar{D}_p$  is the mean electrical mobility diameter of the particle with the nonvolatile salt coating (actual size measured).  $\bar{D}_{p,\text{salt}}$  was  $11.88 \text{ nm} \pm 0.07 \text{ nm}$  for RM30 and  $12.38 \text{ nm} \pm 0.07 \text{ nm}$  for RM60 based on these dilution conditions. These measurements were also calibrated by SRM 1964 as described later.

### Calibration using standard artifact

The mode of the number distribution of SRM 1964, PSL particles with a certified diameter of 60.39 nm and a combined standard uncertainty of 0.31 nm, was used to calibrate DMA for step mode and scan mode. The calibration was based on the direct proportionality between mobility and flow (Equation (2)) as given in Equation (12):

$$q_{\text{cal}} = q_{\text{sh}} \frac{Z_{p,\text{theoretical}}}{Z_{p,\text{experimental}}} \quad (12)$$

where  $q_{\text{cal}}$  is the calibrated sheath flow,  $q_{\text{sh}}$  is the experimental sheath flow,  $Z_{p,\text{theoretical}}$  is the expected mobility of the calibrant, and  $Z_{p,\text{experimental}}$  is the measured mobility of the calibrant. The quantity  $q_{\text{cal}}$

is the value of the sheath flow that gives the correct mobility. Measurements of the mobility distribution (voltage vs. number concentration) were sufficient to determine the mode and calibrate the sheath flow in previous studies with alternative size standards (e.g., SRM 1964 and SRM 1963a certified by SRM 1963). However, in this case for SRM 1964, we found that the mode of the mobility distribution corresponded to a size about 0.2 nm smaller than the certified mode in the diameter distribution. This means that the mode of the mobility distribution does not exactly correspond to the mode of the diameter distribution, likely due to the relatively broad size distribution of SRM 1964. As a result, a correction was applied to shift the mode of the diameter distribution to the certified value. Others have previously computed a corrected flow rate using calibration particles (Wiedensohler et al. 2018). Their approach was only applied to measurements in the step mode. Two values of  $q_{\text{cal}}$  were used to calculate two mode diameters  $D_{p,1}$  and  $D_{p,2}$ , and then the correct sheath flow,  $q_{\text{cal,correct}}$  was calculated using Equation (13).

$$q_{\text{cal,correct}} = q_{\text{cal,1}} + \left( \frac{q_{\text{cal,2}} - q_{\text{cal,1}}}{D_{p,2} - D_{p,1}} \right) (D_{p,\text{cert}} - D_{p,1}) \quad (13)$$

where  $D_{p,\text{cert}}$  is  $60.39 \text{ nm} \pm 0.63 \text{ nm}$  in this case. Any two values near the correct sheath flow can be used. The sheath flow from the mode of the mobility distribution can be used for  $q_{\text{cal,1}}$ . Solve Equation (3) for  $q_{\text{sh}}$  given the certified diameter of SRM 1964 (60.39 nm) and the mode of the mobility distribution ( $V$ ). We arbitrarily set  $q_{\text{cal,2}}$  equal to a value 1% smaller than  $q_{\text{cal,1}}$ . The approximation works best for small differences between  $q_{\text{cal,1}}$  and  $q_{\text{cal,2}}$ , as it assumes a linear relationship between diameter and sheath flow.  $D_{p,1}$  and  $D_{p,2}$  are the modes of the SRM 1964 distributions corresponding to  $q_{\text{cal,1}}$  and  $q_{\text{cal,2}}$ , respectively. The modes were determined by applying a sheath flow to a mobility distribution data set: Equation (3) was used to convert voltage to diameter and Equation (7) was used to convert  $N_{\text{CPC}}$  to  $dN/dD_p$ . The modes were calculated by applying cubic fits to all points where the  $y$ -axis signal was greater or equal to half the maximum  $y$ -axis signal ( $N_i \geq 0.5 N_{\text{max}}$ ). The derivatives of the cubic fits were set to zero and the roots were solved for using the quadratic equation.

### Calibration using DryCal

The sheath flow was measured by the external TSI mass flow meter, which was calibrated using the

DryCal (Model Defender 530, Mesa Labs, Butler, NJ, USA). The test sheath flow was set by the MKS mass flow controller to various values bracketing the desired flow rate of  $5.9 \text{ standard L min}^{-1}$  to  $6.2 \text{ standard L min}^{-1}$ . The standard conditions of the flow meter were 294.26 K and 101.3 kPa. Twenty measurements of the flow rate were made with the DryCal at each test flow rate, and a correction was applied to the TSI flow meter measurement. The DryCal measurement ranged from 0.07% to 0.97% higher than the TSI flow meter measurement and has a volumetric accuracy of 0.75%. The TSI flow meter was subsequently used to calibrate the recirculating flow of the SMPS.

### Experimental design

The size distributions of four samples (unique 1 mL aliquots) were measured from a combined source (four 5 mL ampules) on a single day. Four calibration measurements (SRM 1964) were made on a single sample to allow the determination of the peak voltage (a different sample was prepared each day for three total SRM 1964 samples). This did not require the entire size distribution to be measured, as the mode can be determined without measuring from baseline to baseline. The repeat calibrant measurements were made to correct for drift over the 15 min measurement time. The same measurement sequence was repeated on two other days to assess the effect of day-to-day variability on the average particle size. The measurement sequence is shown in Table 2. This process was used for both RM30 (nominal 30 nm gold nanoparticles) and RM60 (nominally 60 nm). This method was followed for step measurements and independently for SMPS measurements on a different series of three days. The step-voltage data was calibrated by SRM 1964, while the SMPS raw data was calibrated by two independent methods for comparison: SRM 1964 and the DryCal.

### Uncertainty analysis

An uncertainty analysis includes a Type A component that can be calculated by statistical means, such as the standard deviation of a set of measurements, and a Type B component that is calculated by other means such as uncertainties assigned to reference data.

The Type A uncertainty was determined by analyzing the means and standard deviations of replicate measurements performed over three days using the DerSimonian–Laird approach (DerSimonian and Laird

1986). Only the Type A uncertainty is presented for the SMPS measurements because a full uncertainty budget has not been determined. The DerSimonian–Laird approach is a random effects model that expresses each measured value  $D_{p,j}$  as an additive superposition of three elements:

$$D_{p,j} = \psi + \theta_j + \varepsilon_j \quad (14)$$

where  $\psi$  is the measurand (true value of  $D_p$ ),  $\varepsilon_j$  refers to the measurement uncertainty, and  $\theta_j$  to the day-to-day variation. The variance of the day-to-day effect is  $\tau^2$ . The quantity  $\varepsilon_j$  is assumed to be an independent random variable with variance  $\sigma_j^2$ , which is estimated as the variance of the four mean diameter measurements on day  $j$ ,  $u_j^2$ . The estimated value of the mean diameter,  $\hat{D}_{p,avg}$ , is given by the following expression:

**Table 2.** The experimental design of the step-voltage and SMPS measurements of the AuNPs (Samples A through L).

Test Day	Test ID	Calibrant used
Day 1	SRM 1964 1	–
	Sample A	SRM 1964 1
	Sample B	SRM 1964 2
	SRM 1964 2	–
	SRM 1964 3	–
	Sample C	SRM 1964 3
	Sample D	SRM 1964 4
	SRM 1964 4	–
Day 2	SRM 1964 5	–
	Sample E	SRM 1964 5
	Sample F	SRM 1964 6
	SRM 1964 6	–
	SRM 1964 7	–
	Sample G	SRM 1964 7
	Sample H	SRM 1964 8
	SRM 1964 8	–
Day 3	SRM 1964 9	–
	Sample I	SRM 1964 9
	Sample J	SRM 1964 10
	SRM 1964 10	–
	SRM 1964 11	–
	Sample K	SRM 1964 11
	Sample L	SRM 1964 12
	SRM 1964 12	–

The samples are aliquots in unique microcentrifuge tubes.

$$\hat{D}_{p,avg} = \frac{\sum_{j=1}^3 w_j \bar{D}_{p,j}}{\sum_{j=1}^3 w_j} \quad (15)$$

where  $\bar{D}_{p,j}$  is the average of the four mean diameter measurements on the  $j$ th day and with weights given by:

$$w_j = 1/(\tau^2 + u_j^2) \quad (16)$$

Since the value of  $\tau$  is not known, it is replaced with a method of moments estimate provided Equation (17) gives a non-negative result:

$$\hat{\tau}^2 = \frac{(Q - m + 1)}{\sum_{j=1}^3 u_j^{-2} - \sum_{j=1}^3 u_j^{-4} / \sum_{j=1}^3 u_j^{-2}} \quad (17)$$

where

$$Q = \sum_{j=1}^3 u_j^{-2} (\bar{D}_{p,j} - \hat{D}_{p,avg})^2 \quad (18)$$

$m$  is the number of days. If this results in a negative value of  $\hat{\tau}^2$ , one sets  $\hat{\tau}^2 = 0$ . The initial estimate of  $\hat{D}_{p,avg}$  is taken to be the average of all twelve diameter measurements. One does a successive iteration of this calculation if the value of  $\hat{D}_{p,avg}$  computed via Equation (15) differs from the initial estimate. The standard uncertainty in the value of  $\hat{D}_{p,avg}$  (Higgins, Thompson, and Spiegelhalter 2009) is given by:

$$u_{\hat{D}_{p,avg}} = \sqrt{1 / \sum_{j=1}^3 w_j} \quad (19)$$

The number of degrees of freedom is 2 and the results are summarized in Table 3.

The Type A uncertainty is larger for the SMPS DryCal calibration than for the SMPS particle calibration, though both use the same raw data. One possibility is that the DryCal flow is incorrect because of the meter itself, or because of an unidentified pressure drop in the system. A second possibility is that there is an issue unrelated to the sheath flow that is compensated by the calibration particles. There is a need

**Table 3.** The Type A uncertainties for the step-voltage mode and SMPS measurements.

			$D_{p,avg}$ , nm	$u_{D_{p,avg}}$ , nm	$u_r$ , %
Step-voltage particle calibration	RM30	Without salt correction	33.42	0.10	0.308
	RM30	With salt correction	32.91	0.11	0.327
	RM60	Without salt correction	64.41	0.11	0.163
SMPS particle calibration	RM60	With salt correction	64.25	0.11	0.164
	RM30	Without salt correction	33.69	0.05	0.148
	RM30	With salt correction	33.18	0.05	0.151
SMPS DryCal calibration	RM60	Without salt correction	64.48	0.23	0.364
	RM60	With salt correction	64.32	0.23	0.364
	RM30	Without salt correction	33.03	0.14	0.411
	RM30	With salt correction	32.50	0.14	0.444
	RM60	Without salt correction	63.69	0.41	0.647
	RM60	With salt correction	63.53	0.41	0.644

The data used to calculate the “with salt correction” values are plotted in Figures 7 and 8.

for additional study of the day-to-day and within day variation in DMA and SMPS measurements to reduce the Type A uncertainty.

Type B uncertainties are generally systematic and are characterized by analyzing components of the measurement system. The Type B uncertainty was computed for the step-voltage mode but not for the SMPS measurements because a full uncertainty budget has not been determined for the SMPS. The major contributions to the Type B uncertainty are given in Table 4. The Type B uncertainty for the particle standard calibration method is derived from Equation (20) and follows the method of Mulholland et al. (2006).

$$D_p = \frac{C_c}{C_{c,s}} \frac{V}{V_s} D_{p,s} \quad (20)$$

where  $D_p$  is the particle diameter,  $C_c$  is the slip correction,  $V$  is the voltage, and the additional “s” subscript refers to the size standard, SRM 1964. The final form of the uncertainty expression is given in Equation (21). This expression is derived by first computing the differential  $dD_p$  as a function of the differentials of the variables  $D_{p,s}$ ,  $C$ ,  $C_s$ ,  $V$ , and  $V_s$ . Then the slip correction is expressed as a function of  $T$ ,  $P$ ,  $D_p$ , and a simplified form:  $A$  (Mulholland et al. 2006). The variance of the sum of the differentials is the sum of the individual variances except for the terms  $A$  and  $A_s$ , which are correlated. For example, if the calibration diameter and the unknown diameter

**Table 4.** Relative uncertainty values for significant contributions to particle diameter Type B uncertainty for step mode measurements.

Quantity	Value	Relative uncertainty (%)
Voltage		
SRM 1964	1,400 V	0.06
RM60	1,500 V	0.06
RM30	450 V	0.12
Salt particles	250 V	0.09
Slip correction		
SRM 1964		0
RM60		0.04
RM30		0.35
RM60 salt		0.69
RM30 salt		0.71
Pressure	101.33 kPa	0.22
Temperature	296.15 K	0.20
SRM 1964 diameter	60.39 nm	0.51

**Table 5.** Uncertainty propagation for AuNP diameter determination. Terms 1 through 6 refer to the quantities within parenthesis in Equation (21). The uncertainty propagation for the salt particle diameter is discussed in the Supplemental Information. The uncertainty of the salt corrected AuNP diameter is calculated by Equation (25).

$\bar{D}_p$ , nm	$C_c$	Term 1 $D_p$ for SRM	Term 2, $V$	Term 3, $V$ for SRM	Term 4, $A$	Term 5, $T$	Term 6, $P$	$u_r(\bar{D}_p)$ , %	$u_r(\bar{D}_{p,salt})$ , %	$u_r(\bar{D}_{p,c})$ , %
33.42	7.21	0.486	0.064	0.032	0.162	0.013	0.011	0.518	0.582	0.543
64.41	4.06	0.516	0.034	0.034	0.017	1.9 E-3	1.6 E-3	0.518	0.577	0.522

are the same, then the measurement of the unknown would have no error for the term  $A$ . We estimate the effect of the entire Cunningham slip correction,  $C_c = 1 + Kn(A)$  by computing an unknown diameter based on a fixed calibration diameter (a fixed voltage ratio) but with two different choices of the slip correction factor.

$$u_r^2(D_p) = \left( \frac{f_1(C_{c,s})}{f_1(C_c)} u_r(D_{p,s}) \right)^2 + \left( \frac{1}{f_1(C_c)} u_r(V) \right)^2 + \left( \frac{1}{f_1(C_c)} u_r(V_s) \right)^2 + (u_r(A, A_s))^2 + \left( \frac{f_2(C_c) - f_2(C_{c,s})}{f_1(C_c)} \left( 2 - \frac{T}{T + 110.4 \text{ K}} \right) u_r(T) \right)^2 + \left( \frac{f_2(C_c) - f_2(C_{c,s})}{f_1(C_c)} u_r(P) \right)^2 \quad (21)$$

where  $u_r$  refers to the relative standard uncertainty (%) of the various terms,  $f_1(C_c) = \frac{2C_c-1}{C_c}$ ,  $f_2(C_c) = \frac{C_c-1}{C_c}$ ,  $T$  is the temperature in Kelvin, and  $A$  is a portion of the slip correction as defined in Equation (22).

$$A = \alpha + \beta \exp\left(\frac{-\gamma D_p}{2\lambda}\right) \quad (22)$$

where  $\alpha$ ,  $\beta$ , and  $\gamma$  are empirical constants for the slip correction and  $\lambda$  is the mean free path of the gas. The two sets of coefficients for  $\alpha$ ,  $\beta$ , and  $\gamma$  listed above were used to calibrate and solve for the mean diameter of a data set. The difference between the two means was used to approximate  $u_r(A)$ . The uncertainty associated with each of the six terms in Equation (21) and the overall Type B uncertainty in  $D_p$  are given in Table 5. In the text below, the method for determining the uncertainty in the various components is discussed.

### Voltage

Two power supplies were used to apply the voltage to the DMA column inner rod, one for the step-voltage measurements and one for the SMPS. The power supplies were independently calibrated by connecting the power supply to a Spellman HUD-100-1 precision

resistor ladder and an Agilent 34401A 6.5 digital multimeter. The calibration of the step-voltage power supply corrected the voltage to within 0.14%, combining in quadrature the uncertainty of the multimeter, the resistor ladder, and the residuals of calibration function. The calibration of the SMPS power supply was conducted using Firmware commands within the AIM software and corrected the voltage to within 0.05%. SVO commands were sent to the CPC and then the actual voltage was measured with the multimeter and resistor ladder.

### Pressure

The barometric pressure was measured using a TSI Model 4043 mass flow meter. The stated pressure uncertainty was 1 kPa with traceability to NIST. Additional calibration measurements were made at NIST in the Ultrasonic Interferometer Manometer Lab by comparing the mass flow meter pressure reading to a calibrated Ruska model 6200 pressure gauge at ambient pressure. The accuracy of the pressure gauge is better than 0.05% of the reading or 0.05 kPa at atmospheric pressure. The flow meter read between 100.2 kPa and 100.3 kPa whereas the pressure gauge read 100.33 kPa. We estimate that the TSI flow meter measures within  $\pm 0.2$  kPa of the true pressure. During the step-voltage experiments, the pressure is measured in the excess aerosol tube after the DMA column. For step-voltage measurements, the pressure within the characterization region of the DMA column was determined to be 1.8 kPa  $\pm$  0.1 kPa higher than the TSI meter reading due to internal pressure drops. This pressure was added to the pressure measured during the experiment. The pressure has a relative combined standard uncertainty of 0.22% near ambient pressure. The measurements were made before and after a size distribution measurement was performed, and the average of the two values was used in later calculations. For the SMPS measurements, a single measurement of the pressure is made at the start of the size distribution scan.

### Temperature

The temperature was measured with TSI Model 4043 mass flow meter. The stated temperature uncertainty was 1 °C with traceability to NIST. Additional calibration measurements were made at the NIST Primary Flow Calibration Facility. The temperature was measured to a standard uncertainty of  $\pm 0.02$  K

both before and after the flow meter. The temperature increased from 297.1 K to 298.0 K as the 160 cm<sup>3</sup> s<sup>-1</sup> flow passed through the flow meter, which recorded a reading of 297.4 K. We estimate that the true value of the gas temperature is within  $\pm 1.0$  K of the value measured with the TSI instrument. Assuming a uniform rectangular distribution for the probability distribution of the temperature, we obtain a standard uncertainty in  $T$  equal to  $1/\sqrt{3} = 0.58$  K or a relative standard uncertainty of 0.20% based on a gas temperature of 296.15 K. The drift in temperature during a voltage scan, less than 0.1 K, is small compared to the uncertainty from the calibration and is neglected. For step-voltage measurements, the temperature was measured at the excess flow outlet of the DMA column. The measurements were made before and after a size distribution measurement was made, and the average of the two values was used in later calculations. For the SMPS measurements, a single measurement of the temperature is made at the start of the size distribution scan.

### Particle charging

For a RM30 distribution from 27 nm to 40 nm, the charging probability as a function of diameter given by Equation (6) is well approximated by a linear dependence with slope of 0.0029. The number mean diameter was computed for this value and for a value of 0.0025 for comparison. This decrease in slope is similar to the difference obtained by Li, Chahl, and Gopalakrishnan (2020) for results obtained using Langevin dynamics (Figure 10A) versus Equation (6) (Li, Chahl, and Gopalakrishnan 2020). The resulting difference in the number mean diameter is negligible: 33.092 nm for Equation (6) and 33.088 nm for Langevin Dynamics. Therefore, the uncertainty of the particle charging probability was not included in the uncertainty analysis of the mean diameter. Generally, the particle charging is important for total number concentration calculations and to represent broad distributions accurately. In this case, we are working with relative concentration measurements and narrow size distributions.

### Combined uncertainty

The Type A and Type B uncertainties calculated above were combined by adding the standard uncertainties in quadrature as shown in Equation (23).

**Table 6.** The combined standard and expanded uncertainty values for the step-voltage measurements of the aerosolized particle (no salt correction).

$\bar{D}_p$ , nm	Type B $u_r(\bar{D}_p)$ , %	Type A $u_r(\bar{D}_p)$ , %	Combined $u_r(\bar{D}_p)$ , %	Degrees of freedom	Coverage factor	Combined expanded uncertainty $U_r(\bar{D}_p)$ , %
33.42	0.518	0.308	0.602	27	2.05	1.23
64.41	0.518	0.163	0.543	94	1.99	1.08

**Table 7.** The combined standard and expanded uncertainty values for the step-voltage measurements of the particle in suspension (including salt correction).

$\bar{D}_{p,c}$ , nm	Type B $u_r(\bar{D}_{p,c})$ , %	Type A $u_r(\bar{D}_{p,c})$ , %	Combined $u_r(\bar{D}_{p,c})$ , %	Degrees of freedom	Coverage factor	Combined expanded uncertainty $U_r(\bar{D}_{p,c})$ , %
32.91	0.543	0.327	0.634	26	2.06	1.31
64.25	0.522	0.164	0.547	95	1.99	1.09

$$u_{r, \text{ combined}} = \sqrt{u_{r, \text{ Type A}}^2 + u_{r, \text{ Type B}}^2} \quad (23)$$

The final uncertainty results are expressed in terms of the expanded relative uncertainty (95% confidence interval),  $U_r$ , which is computed from a coverage factor,  $k$ , times the combined standard uncertainty. The value of  $k$  depends on the number of degrees of freedom and can be determined from the critical value table of Student's  $t$  distribution. In the limit of an infinite number of degrees of freedom,  $k = 1.96$  and increases to a value of 2.23 for 10 degrees of freedom. The degrees of freedom are calculated using the Welch-Satterthwaite formula (Satterthwaite 1946) which includes the Type A uncertainty and degrees of freedom, and the degrees of freedom of the calibration standard.

$$v_{\text{eff}} = \frac{u_r^4(D_p)}{\sum_{i=1}^N \frac{c_i^4 u_{r,i}^4(D_p)}{v_i}} = \frac{u_{r, \text{ com, AuNP}}^4}{\frac{u_{r, \text{ A, AuNP}}^4}{2} + \frac{u_{r, \text{ B, SRM}}^4}{123}} \quad (24)$$

where  $u_{r, \text{ com, AuNP}}$  is the relative combined uncertainty of the AuNP,  $u_{r, \text{ A, AuNP}}$  is the Type A relative uncertainty of the AuNP, and  $u_{r, \text{ B, SRM}}$  is the Type B relative uncertainty of the AuNP derived from the calibrant (Term 1 of Table 5). There are 2 degrees of freedom for the Type A uncertainty of the AuNP and 123 degrees of freedom for the calibrant (Mulholland et al. 2006). The values used for these terms are included in Tables 5–7.

The expanded relative uncertainties (95% confidence interval) for the aerosol are given in Table 6 and are between 1% and 1.5%. Corresponding results for the particles in suspension are given in Table 7. The mean diameter of the particles in suspension,  $\bar{D}_{p,c}$ , is given by Equation (11) and the Type B uncertainty in this diameter is given by Equation (25):

$$u_r(\bar{D}_{p,c}) = \left[ \left( \frac{\bar{D}_p}{\bar{D}_{p,c}} \right)^6 u_r(\bar{D}_p)^2 + \left( \frac{\bar{D}_{p, \text{ salt}}}{\bar{D}_{p,c}} \right)^6 u_r(\bar{D}_{p, \text{ salt}})^2 \right]^{1/2} \quad (25)$$

This expression is derived by the law of propagation of uncertainty for the case of two independent variables (based on the relationship in Equation (11)). The uncertainty components of the salt particles are included in the Supplemental Information.

## Results

Forty-eight total measurements were conducted on RM30 and RM60. Of these, 12 were made on RM30 in the step-voltage mode, 12 of RM30 were made with the SMPS, 12 of RM60 were made in the step-voltage mode, and 12 were made on RM60 with the SMPS. Each set of 12 measurements was made over three days, i.e., four per day. The SMPS data were calibrated by two methods: using the known size of a certified size standard (artifact) to calibrate the sheath flow or using the DryCal to calibrate the sheath flow measured by the external flow meter. Each method additionally required accurate knowledge of the voltage, temperature, and pressure. Representative scanning electron microscopy (SEM) images of the particles are included in Figures 3 and 4.

Method testing was done using a commercial batch of 60 nm AuNPs from Ted Pella. As shown in Table 8, minimal change (relative to the standard deviation) was observed above 150 s scan up time at the given measurement conditions (6 L min<sup>-1</sup> sheath flow, 50 nm to 85 nm scan, 16 data points). For the DryCal flow calibration, the measured mean particle size decreased by 1.6% as the scan time was reduced to 30 s while for the particle calibration method the

change was 0.3%. The effect is smaller for the particle calibration method because both the size standard and the unknown particle size measurements are biased to

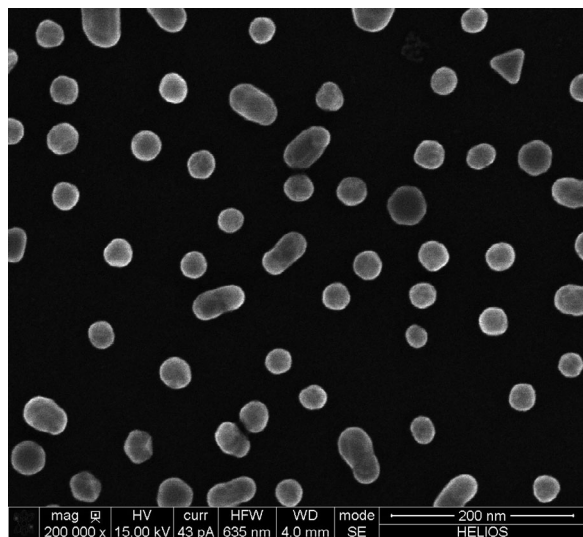


**Figure 3.** Representative SEM image of RM30 at  $\times 200,000$  magnification on a Si/SiO substrate. The primary particles are somewhat aspherical with faceted edges and include a small population of asymmetric shapes.

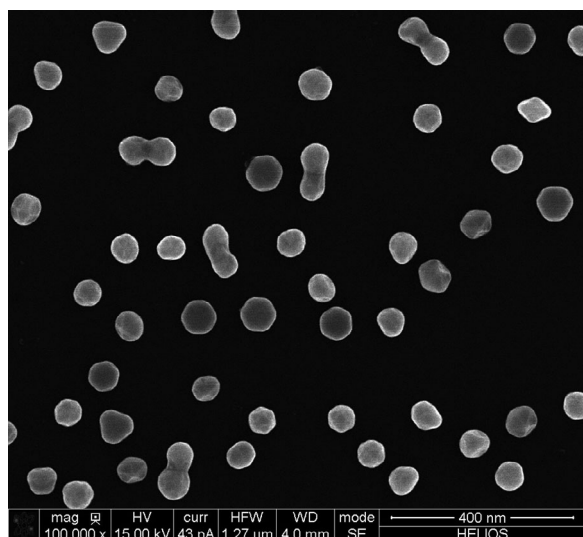


**Figure 4.** Representative SEM image of RM60 at  $\times 100,000$  magnification on a Si/SiO substrate. The primary particles are somewhat aspherical with faceted edges and include a small population of asymmetric shapes.

smaller size. We note that other documentations of the scan speed issue report an increase in mean particle size with an increase in scan speed (Tokonami and Knutson 2000).

In addition, the delay time ( $t_d$ ) was studied for the same test particles with results presented in Table 9. Various  $t_d$  values were used in the AIM software and the mean size was measured. Even large changes in the delay time show minimal effect on the measured mean diameter for the given measurement settings ( $6 \text{ L min}^{-1}$  sheath flow, 50 nm–85 nm scan, 16 data points, 300 s scan up, 30 s scan down). Minimizing the scan range significantly reduces the error associated with an incorrect delay time.

The average size distributions for RM30 and RM60 by each calibration technique are presented in Figures 5 and 6, and the compiled mean diameter measurements are shown in Figures 7 and 8. The distribution measured by the SMPS calibrated by the particle size standard is slightly shifted (0.4 nm) to larger size relative to the step-voltage measurements for RM30 (Figure 5). The percent shift is about a factor of two smaller for RM60. However, some minor differences were seen for the measurements of RM60 (Figure 6). For the step-voltage method, the background is slightly higher, and a minor secondary peak was reproducibly detected at 72 nm.

The blue and orange data in Figures 7 and 8 require two sets of data each over a longer period of time than the SMPS measurements with DryCal calibration. This could be responsible for the larger within day drift for these data sets. Day-to-day variability in ambient conditions (temperature, pressure, and humidity) may be responsible for the larger day-to-day drift of the SMPS with DryCal calibration. Even though the flow meter is corrected with the DryCal, the precision and accuracy of these

**Table 9.** Effect of delay time ( $t_d$ ) on mean particle size of 60 nm AuNPs by SMPS.

Delay time (s)	Mean diameter (nm)
3.33	64.06
3.43	64.11
3.53	64.01
4.00	63.97
6.00	63.90

**Table 8.** Effect of scan time on mean particle size by SMPS.

		Mean or mode diameter (nm) at given scan time		
		30 s	150 s	300 s
Particle calibration	Uncalibrated SRM 1964 mode	59.56	60.80	60.85
	Uncalibrated AuNP mean	63.22	64.61	64.72
	Calibrated AuNP mean	63.87	63.82	63.78
DryCal calibration	Calibrated AuNP mean	62.29	63.27	63.44

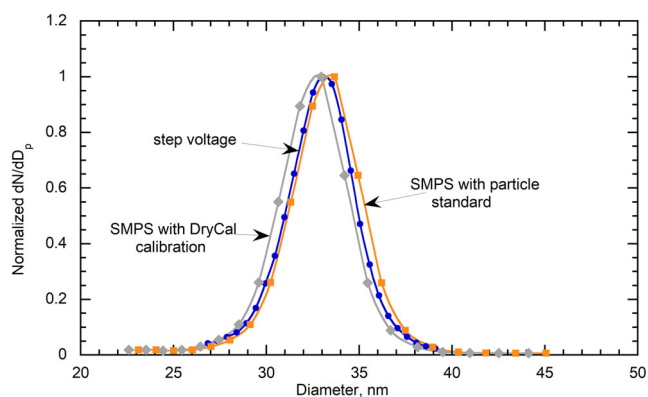


**Figure 5.** Average normalized size distributions of RM30. The (blue) circles are step-voltage measurements, the (orange) squares are SMPS measurements with size standard calibration, and the (gray) diamonds are SMPS measurements with DryCal calibration. The (orange) squares and (gray) diamonds lines use the same raw data with different calibrations. The size was corrected for the aerosol salt coating.

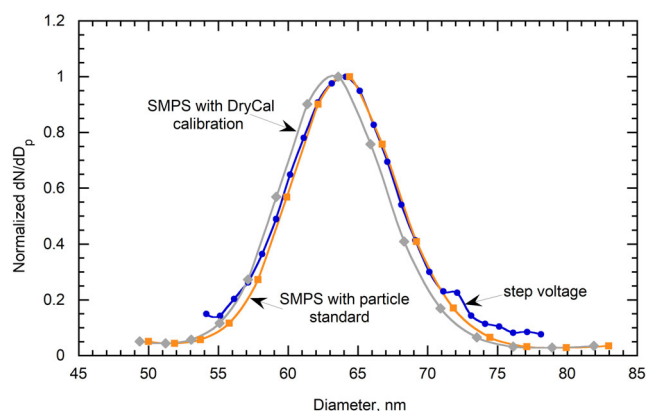


**Figure 6.** Average normalized size distributions of RM60. The (blue) circles are step-voltage measurements, the (orange) squares are SMPS measurements with size standard calibration, and the (gray) diamonds are SMPS measurements with DryCal calibration. The (orange) squares and (gray) diamonds lines use the same raw data with different calibrations. The size was corrected for the aerosol salt coating.

corrections are on the order of 0.5%. Another possibility is that the change in ambient conditions affects other operating conditions such as the aerosol flow or the operation of the electrospray.

The mean diameter from the DerSimonian–Laird estimator for the scan-voltage measurements was calibrated by SRM 1964, and SMPS measurements calibrated by the DryCal agreed with the step-voltage value are detailed in Table 10 within the expanded uncertainty (95% confidence interval) of the measurement. The data were presented with and without the salt correction (aerosol indicates the size of the aerosolized particle with a salt coating). The salt correction (Equation (11)) was kept constant for the three

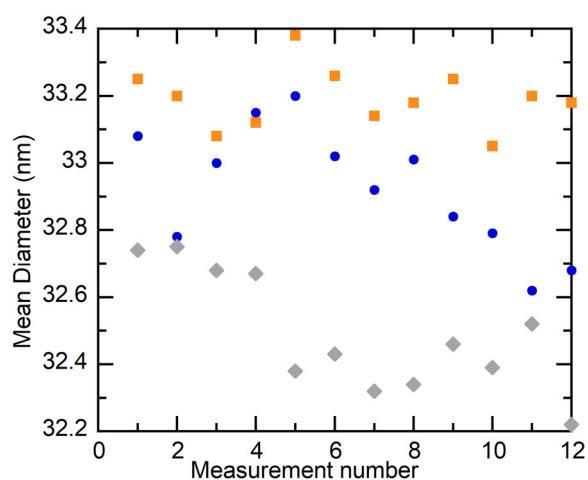


**Figure 7.** Repeat measurements of RM30 over six days. The (blue) circles are step-voltage measurements, the (orange) squares are SMPS measurements with size standard calibration, and the (gray) diamonds are SMPS measurements with DryCal calibration. The (orange) squares and (gray) diamonds points use the same raw data with different calibrations. The size was corrected for the aerosol salt coating.

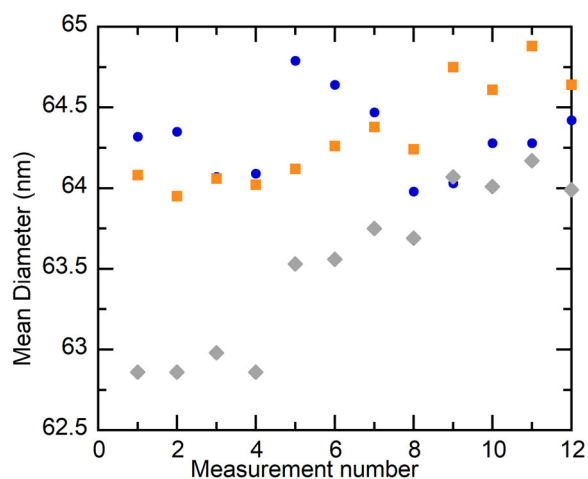


**Figure 8.** Repeat measurements of RM60 over six days. The (blue) circles indicate step-voltage measurements, the (orange) squares indicate SMPS measurements with size standard calibration, and the (gray) diamonds indicate SMPS measurements with DryCal calibration. The (orange) squares and (gray) diamonds points use the same raw data with different calibrations. The size was corrected for the aerosol salt coating.

measurement approaches to limit variables. The measurement of the salt is simpler when using the SMPS, because a rapid test measurement can be made over the entire size distribution to identify the salt region and particle of interest region.

One limitation of the SMPS is that the  $x$ -axis spacing is preset in the software. For a very narrow particle distribution, additional data points cannot be added over a given size range. This comparison is illustrated in Figure 9, where the  $x$ -axis spacing is set

**Table 10.** Mean diameter from the DerSimonian-Laird estimator of RM30 and RM60 for various measurement and calibration techniques with and without salt correction for aerosolized particles.

		Mean diameter (nm)	
		RM30	RM60
Step-voltage particle calibration	Without salt correction	33.42 ± 0.41	64.41 ± 0.70
	With salt correction	32.91 ± 0.43	64.25 ± 0.70
SMPS particle calibration	Without salt correction	33.69 ± 0.05	64.48 ± 0.23
	With salt correction	33.18 ± 0.05	64.32 ± 0.23
SMPS DryCal calibration	Without salt correction	33.03 ± 0.14	63.69 ± 0.41
	With salt correction	32.50 ± 0.14	63.53 ± 0.41

The uncertainty for the step-voltage particle calibration data is the expanded combined Type A and Type B uncertainty with a coverage factor,  $k$ , ranging from 1.99–2.06 (95% confidence interval). Only the standard Type A uncertainty is included in the calculation for the SMPS particle calibration and SMPS DryCal calibration.

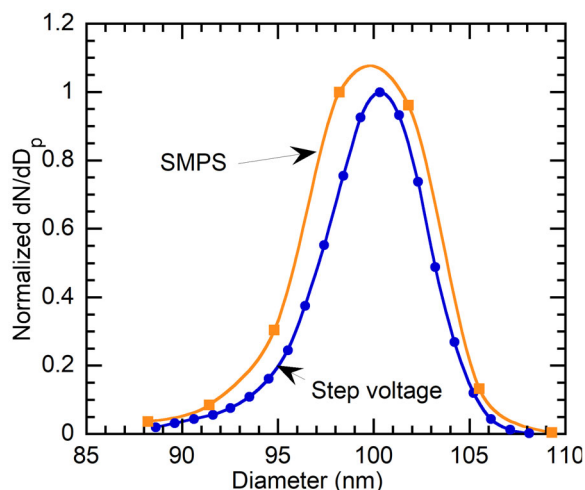


**Figure 9.** Size distribution of SRM 1963a measured by step-voltage mode (blue circles) and SMPS with DryCal calibration (orange squares).

much narrower in the step-voltage mode, which allows for improved peak definition (specifically for determining the mode) of the narrow size distribution of nominally 100 nm SRM 1963a.

Table 11 illustrates differences between size measurements with all variables kept constant except for the method of voltage change. These measurements were made within a single day, alternating between step-voltage mode and SMPS, thus day-to-day variability was eliminated and any change with time should affect both measurements equally. We found a bias of  $\approx 0.5$  nm between the step-voltage and SMPS measurements for the mean diameters of RM30 and RM60, and a bias of  $\approx 0.3$  nm for the mode diameter of SRM 1964. Having controlled for all other relevant variables, we believe this difference is due to differences in voltage control: step-mode vs. scan-mode.

## Discussion

The difference of 0.27 nm between the DerSimonian-Laird mean aerosol diameters by step-

voltage and SMPS calibrated by SRM 1964 for RM30 was smaller than the expanded uncertainty (95% confidence interval). The difference of 0.07 nm for RM60 was much smaller than the standard uncertainty, partly because the calibration particle size and the AuNP size were both nominally 60 nm. The difference of 0.39 nm between the mean diameters by step-voltage and SMPS calibrated by the DryCal for RM30 was on the order of the expanded uncertainty (95% confidence interval). The difference of 0.72 nm for RM60 was also on the order of the expanded uncertainty. Calibration with the DryCal is the recommended method by TSI and generally works well within a few percent of the step-voltage data. This is likely sufficient for most purposes but was less accurate than the calibration method using the size standard for calibration.

Mai and Flagan (2018) pointed out the potentially large error in sizing with the SMPS if one used the instantaneous voltage of the particle leaving the DMA column, rather than the voltage averaged over the time interval that the particle is in the classification region. It is not clear from correspondence with TSI whether the software for analyzing the SMPS data (AIM 9.0.0.0) uses the average voltage described earlier, a different average, or the instantaneous voltage when the particle is at the outlet. We have compared the first and last approaches using a 300 s scan time and a 3.94 s delay time and show in the Supplemental Information that the diameter computed by the average voltage is 0.46% smaller for RM30 and 0.33% smaller for the RM60 than the diameter computed by the voltage corresponding to when the particle leaves the DMA column. These values are about 2/3 of the relative combined uncertainties for these particle sizes and so is a minor effect. Also, the effect is in the opposite direction for the above observed relationship between SMPS and step-voltage, where the SMPS measured a larger size for the 30 nm particles. The effect is small because the scan time is long, but the

**Table 11.** Mean of mean diameters of RM30 and RM60 by uncalibrated measurements using the same sheath flow alternating between step-voltage mode and SMPS.

Measurement Method		Mean diameter (nm)		Mode diameter (nm)
		RM30	RM60	SRM 1964
Step-voltage	Without salt correction	34.55 ± 0.09	65.80 ± 0.20	63.09 ± 0.24
SMPS	Without salt correction	34.13 ± 0.14	65.20 ± 0.27	62.83 ± 0.35

The uncertainty is one standard deviation of 9 (RM30) or 8 measurements (RM60).

effect becomes important for short scan times (such as a 5.2% reduction in size for a 30-s time scan for the 30 nm particle size).

One challenge in this study was the lack of information about the algorithm used in the analysis of the SMPS data. Specifically, it was unclear what voltage was being reported by the software: the average voltage experienced by a particle going through the DMA column or the voltage when the particle exited the DMA column. This issue could be resolved by developing a widely accessible open access code for analyzing the data. Such a code, with details regarding the treatment of the voltage, would be helpful in assessing whether the 0.5 nm smaller size measured by the scan mode in the uncalibrated measurements shown in Table 10 is from the voltage analysis.

Mai and Flagan (2018) and Mai et al. (2018) used Brownian dynamics simulations to find the instantaneous transfer function of the SMPS based on the flow field and electric field obtained from finite element simulations of the actual geometry of the DMA column being studied (TSI Model 3081 DMA long-column). Losses and time delays in the entrance and exit regions of the DMA column are incorporated into the transfer function, as are losses to the walls of the classification region. In our analysis, the time response of the CPC was assumed to be instantaneous. The time-dependent response has been characterized by a combination of a plug flow, a well-mixed, and a laminar element in the study by Mai and Flagan (Mai et al. 2018). The combined transfer function (including CPC) involves a convolution of the DMA column instantaneous transfer function with the CPC transfer function. Ultimately one obtains the number of particles collected per time bin as function of time. As a result of the well-mixed component of the response time distribution, it is possible to have one particle exit the DMA column earlier, compared to an identical size particle, but to be counted later. This results in a broader combined transfer function and in the case of an up scan (progressively increasing voltage) it shifts the particle mean size to a larger diameter.

In Figure 8 of Mai and Flagan (Mai et al. 2018), there is a comparison of their detailed geometric

model of the transfer function with the prediction of a simplified model, like the one used here, with a Knutson–Whitby type transfer function. For a scan time of 45 s, the peak diameter for the simpler model was 9 nm smaller than the corrected distribution value of 144 nm. Also, for the model that uses the voltage at the time the particle exits the DMA column instead of the average voltage, the diameter is too large by 51 nm. However, for the slow scan rate of 240 s, the Knutson–Whitby approach using the average voltage was 1 nm small while the result that did not use the average voltage was 10 nm large. There is the following quote from Mai et al.: “However, very slow scans allow accurate recovery of the size distribution to be obtained by inversion of measured counts using the idealized, parallel-flow DMA column transfer function, and can be expected to approach that of properly made [step-voltage] measurements” (Mai et al. 2018). Based on this statement and the closeness between the step-voltage and SMPS results, the Type B uncertainty analysis for the uncertainty in the step mode is a good approximation for the Type B uncertainty of the SMPS for the case of a long scan time (300 s) for a diameter sizing range of a factor of 2 (i.e., 25 nm–50 nm) with 64 channels.

The best agreement between step and scan mode in this study resulted from calibration with a particle size standard. An advantage to the particle calibration method is that it can simultaneously correct for the sheath flow and the dimensions of the DMA column. It may also correct for a systematic effect such as a short scan time, since both the known and unknown samples may be affected in the same way. This may account for the constancy of the particle size measured as a function of scan time for the calibrated measurements versus the uncalibrated in Table 8. Also, the uncertainty in the slip correction term is reduced because the diameter of the standard is known. For example, if the unknown particle had the same mobility as the standard, the uncertainty in the slip correction would be zero. Below, a calibration protocol for the SMPS is outlined based on using these AuNPs as future calibrants:

1. Measure the size distribution of calibration particles with a certified mean diameter for given flow conditions.
2. If the number mean diameter does not agree with the certified value, postprocess the data to adjust the sheath flow in the analysis until one obtains the certified diameter. Procedures for doing this are explained in the Supplemental Information.
3. Measure the size distribution of unknown samples.
4. Use the corrected sheath flow (from step 2) to determine the size distribution for the unknown samples by postprocessing the data.

This process works best with the small, monodisperse droplets produced by the electrospray, or by nebulization with minimal nonvolatile material. The SMPS as currently designed, with a maximum of 64 channels per decade, is not applicable to all distributions. Specifically, when it is desirable to determine the mode of the distribution, generally five or more points are required where the  $y$ -axis signal is greater than or equal to half of the maximum  $y$ -axis signal ( $N_i \geq 0.5 N_{\max}$ ). This criterion was narrowly missed for RM30 and RM60 with CVs of 5.1% and 6.8%, respectively. The distributions were sufficient for the calculation of a mean, but a mode would be less well defined. In the case of SRM 1963a (Figure 9), with a CV of 2.6%, the distribution obtained by SMPS is poorly defined for both a mean and a mode. We recommend a minimum CV (for the analyte) of 4% to determine the mean and 8% to determine the mode by SMPS with a 1:20 flow rate ratio.

An additional step was required for the calibration with the certified mode diameter of a particle size standard. Generally, using the mode of the mobility distribution has been sufficient for calibration as it corresponds closely with the mode of the diameter distribution. However, in this case the mode of the mobility distribution (voltage distribution) of SRM 1964 corresponded to a mode of the diameter distribution about 0.2 nm smaller than the certified diameter. A correction was applied to set the sheath flow calibration based on the mode of the diameter distribution rather than the mobility distribution.

The mean diameter was determined using  $dN/d\log D_p$ , though the same calculation can be made using  $dN/dD_p$  instead of  $dN/d\log D_p$ . The mode for SRM 1964 using  $dN/dD_p$  was found to be consistently 0.1 nm larger than that for  $dN/d\log D_p$ . This can be important for the calibration procedure described here because sometimes mode diameters are used for

calibration. It is therefore important to verify how a calibration standard (artifact) was certified. In the present case, SRM 1964 has a certified mode diameter that was determined in the certifying measurements using  $dN/dD_p$ .

## Conclusions

Comparison measurements of 30 nm and 60 nm AuNPs were presented for the DMA operated in step-voltage and scan-voltage modes using a nanoparticle size standard (artifact). The DerSimonian–Laird mean aerosol diameters for the SMPS (33.69 nm and 64.48 nm) agreed within the expanded combined uncertainties (0.43 nm and 0.70 nm) of the step mode measurements (33.42 nm and 64.41 nm). The inferred sizes for the particles in suspension are about 0.5 nm smaller for the 30 nm AuNPs and about 0.2 nm smaller for the 60 nm AuNPs for both measurement modes. Accurately calibrating the sheath flow but not using a particle size standard resulted in undersizing of the particles by nearly the expanded uncertainty (95% confidence interval) in both cases (33.03 nm and 63.69 nm). The use of a calibration particle corrects for the flow and geometric effects, and was found to minimize the effect of a reduced scan time. A methodology was presented for the use of these and other monodisperse calibration particles for accurately calibrating SMPS instruments for the measurement of the mobility diameter distribution. Using such a protocol will improve accuracy, enhance the intercomparison of results from different laboratories, and enable advances in the field of aerosol science. In performing calibration measurements with narrowly distributed reference materials, it was found that the maximum size resolution of 64 size readings per decade was not adequate to determine the mode of the size distribution. The recommended minimum values of the coefficient of variation (one standard deviation divided by the mean) for the measurement of the mode diameter is 8% and for the mean diameter is 4%.

## Acknowledgments

We thank Blaza Toman at NIST for assistance with the Type A uncertainty analysis. The representative SEM images were provided by Dr. Andras Vladar of the NIST Physical Measurements Laboratory.

## Disclosure statement

The authors report there are no competing interests to declare.

## Funding

KD was supported in part by a grant from the National Institute of Standards and Technology, Materials Measurement Science Division (Award No. 70NANB17H057).

## ORCID

Kaleb Duelge  <http://orcid.org/0000-0002-6367-3822>

George Mulholland  <http://orcid.org/0000-0001-7889-3599>

Michael Zachariah  <http://orcid.org/0000-0001-9116-7110>

Vincent A. Hackley  <http://orcid.org/0000-0003-4166-2724>

## References

- Choi, S., C. L. Myung, and S. Park. 2014. Review on characterization of nano-particle emissions and PM morphology from internal combustion engines: part 2. *Int. J. Automot. Technol.* 15 (2):219–27. doi: [10.1007/s12239-014-0023-9](https://doi.org/10.1007/s12239-014-0023-9).
- DerSimonian, R., and N. Laird. 1986. Meta-analysis in clinical trials. *Controlled Clin. Trials* 7 (3):177–88. doi: [10.1016/0197-2456\(86\)90046-2](https://doi.org/10.1016/0197-2456(86)90046-2).
- Dixon, R., R. Koning, V. W. Tsai, J. Fu, and T. V. Vorburger. 1999. Nanometer-scale dimensional metrology with the NIST calibrated atomic force microscope. *Microsc. Microanal.* 5 (Suppl 2):958–9. doi: [10.1017/S1431927600018110](https://doi.org/10.1017/S1431927600018110).
- Duelge, K. J., J. Parot, V. A. Hackley, and M. R. Zachariah. 2020. Quantifying protein aggregation kinetics using electro-spray differential mobility analysis. *J. Pharm. Biomed. Anal.* 177:112845. doi: [10.1016/j.jpba.2019.112845](https://doi.org/10.1016/j.jpba.2019.112845).
- Elahi, N., M. Kamali, and M. H. Baghersad. 2018. Recent biomedical applications of gold nanoparticles: A review. *Talanta* 184:537–56. doi: [10.1016/j.talanta.2018.02.088](https://doi.org/10.1016/j.talanta.2018.02.088).
- Gibson, E. R., P. K. Hudson, and V. H. Grassian. 2006. Aerosol chemistry and climate: Laboratory studies of the carbonate component of mineral dust and its reaction products. *Geophys. Res. Lett.* 33 (13):L13811. doi: [10.1029/2006GL026386](https://doi.org/10.1029/2006GL026386).
- Guha, S., M. Li, M. J. Tarlov, and M. R. Zachariah. 2012. Electrospray-differential mobility analysis of bionanoparticles. *Trends Biotechnol.* 30 (5):291–300. doi: [10.1016/j.tibtech.2012.02.003](https://doi.org/10.1016/j.tibtech.2012.02.003).
- Higgins, J. P. T., S. G. Thompson, and D. J. Spiegelhalter. 2009. A re-evaluation of random-effects meta-analysis. *J. R. Stat. Soc. Ser. A Stat. Soc.* 172 (1):137–59. doi: [10.1111/j.1467-985X.2008.00552.x](https://doi.org/10.1111/j.1467-985X.2008.00552.x).
- Kim, J. H., G. W. Mulholland, S. R. Kukuck, and D. Y. H. Pui. 2005. Slip correction measurements of certified PSL nanoparticles using a nanometer differential mobility analyzer (nano-DMA) for Knudsen number from 0.5 to 83. *J. Res. Natl. Inst. Stand. Technol.* 110 (1):31–54. doi: [10.6028/jres.110.005](https://doi.org/10.6028/jres.110.005).
- Knutson, E. O., and K. T. Whitby. 1975. Aerosol classification by electric mobility: Apparatus, theory, and applications. *J. Aerosol Sci.* 6 (6):443–51. doi: [10.1016/0021-8502\(75\)90060-9](https://doi.org/10.1016/0021-8502(75)90060-9).
- Lamberg, H., O. Sippula, J. Joutsensaari, M. Ihalainen, J. Tissari, A. Lahde, and J. Jokiniemi. 2018. Analysis of high-temperature oxidation of wood combustion particles using tandem-DMA technique. *Combust. Flame* 191: 76–85. doi: [10.1016/j.combustflame.2017.12.027](https://doi.org/10.1016/j.combustflame.2017.12.027).
- Li, L., H. S. Chahl, and R. Gopalakrishnan. 2020. Comparison of the predictions of Langevin Dynamics-based diffusion charging collision kernel models with canonical experiments. *J. Aerosol Sci.* 140:105481. <Go to ISI>://WOS:000505002500003. doi: [10.1016/j.jaerosci.2019.105481](https://doi.org/10.1016/j.jaerosci.2019.105481).
- Mai, H. J., and R. C. Flagan. 2018. Scanning DMA data analysis I. Classification transfer function. *Aerosol Sci. Technol.* 52 (12):1382–99. doi: [10.1080/02786826.2018.1528005](https://doi.org/10.1080/02786826.2018.1528005).
- Mai, H. J., W. M. Kong, J. H. Seinfeld, and R. C. Flagan. 2018. Scanning DMA data analysis II. Integrated DMA-CPC instrument response and data inversion. *Aerosol Sci. Technol.* 52 (12):1400–14. doi: [10.1080/02786826.2018.1528006](https://doi.org/10.1080/02786826.2018.1528006).
- Mulholland, G. W., N. P. Bryner, and C. Croarkin. 1999. Measurement of the 100 nm NIST SRM 1963 by differential mobility analysis. *Aerosol Sci. Technol.* 31 (1):39–55. doi: [10.1080/027868299304345](https://doi.org/10.1080/027868299304345).
- Mulholland, G. W., M. K. Donnelly, C. R. Hagwood, S. R. Kukuck, V. A. Hackley, and D. Y. H. Pui. 2006. Measurement of 100 nm and 60 nm particle standards by differential mobility analysis. *J. Res. Natl. Inst. Stand. Technol.* 111 (4):257–312. doi: [10.6028/jres.111.022](https://doi.org/10.6028/jres.111.022).
- Mulholland, G. W., A. W. Hartman, G. G. Hembree, E. Marx, and T. R. Lettieri. 1985. Development of a one-micrometer-diameter particle-size standard reference material. *J. Res. Natl. Bur. Stand. (1977)* 90 (1):3–26. doi: [10.6028/jres.090.001](https://doi.org/10.6028/jres.090.001).
- Particle Technology Technical Notes and Reference Guide – Strategies and Procedures for Bead Optimization.* 2018. Waltham, MA, USA: ThermoFisher Scientific.
- Satterthwaite, F. E. 1946. An approximate distribution of estimates of variance components. *Biometrics Bull.* 2 (6): 110–14. doi: [10.2307/3002019](https://doi.org/10.2307/3002019).
- Smith, J. N., K. C. Barsanti, H. R. Friedli, M. Ehn, M. Kulmala, D. R. Collins, J. H. Scheckman, B. J. Williams, and P. H. McMurry. 2010. Observations of aminium salts in atmospheric nanoparticles and possible climatic implications. *Proc. Natl. Acad. Sci. USA* 107 (15):6634–9. doi: [10.1073/pnas.0912127107](https://doi.org/10.1073/pnas.0912127107).
- Takahata, K., H. Sakurai, and K. Ehara. 2020. Accurate determination of mass and diameter of monodisperse particles by the electro-gravitational aerosol balance: Correction for the work function imbalance between the electrode surfaces. *Aerosol Sci. Technol.* 54 (12):1386–98. doi: [10.1080/02786826.2020.1787324](https://doi.org/10.1080/02786826.2020.1787324).
- Tokonami, S., and E. O. Knutson. 2000. The scan time effect on the particle size distribution measurement in the scanning mobility particle sizer system. *Aerosol Sci. Technol.* 32 (3):249–52. doi: [10.1080/027868200303786](https://doi.org/10.1080/027868200303786).
- Tsai, D. H., F. W. DelRio, A. M. Keene, K. M. Tyner, R. I. MacCuspie, T. J. Cho, M. R. Zachariah, and V. A. Hackley. 2011. Adsorption and conformation of serum albumin protein on gold nanoparticles investigated using

- dimensional measurements and in situ spectroscopic methods. *Langmuir* 27 (6):2464–77. doi: [10.1021/la104124d](https://doi.org/10.1021/la104124d).
- Wang, S. C., and R. C. Flagan. 1990. Scanning electrical mobility spectrometer. *Aerosol Sci. Technol.* 13 (2): 230–40. doi: [10.1080/02786829008959441](https://doi.org/10.1080/02786829008959441).
- Wiedensohler, A. 1988. An approximation of the bipolar charge distribution for particles in the submicron size range. *J. Aerosol Sci.* 19 (3):387–9. doi: [10.1016/0021-8502\(88\)90278-9](https://doi.org/10.1016/0021-8502(88)90278-9).
- Wiedensohler, A., A. Wiesner, K. Weinhold, W. Birmili, M. Hermann, M. Merkel, T. Müller, S. Pfeifer, A. Schmidt, T. Tuch, et al. 2018. Mobility particle size spectrometers: Calibration procedures and measurement uncertainties. *Aerosol Sci. Technol.* 52 (2):146–64. <Go to ISI>://WOS:000427369900003. doi: [10.1080/02786826.2017.1387229](https://doi.org/10.1080/02786826.2017.1387229).